Heat transfer coefficient retrieval in the impingement jet heat transfer

Arkadiusz Ryfa[1*] and Ryszard Białecki[2]
[1]*Institute of Thermal Technology, Silesian University of Technology*
Konarskiego 22, 44-100 Gliwice, Poland
Arkadiusz.Ryfa@polsl.pl
[2]*Institute of Thermal Technology, Silesian University of Technology*
Konarskiego 22, 44-100 Gliwice, Poland
e-mail: Ryszard.Bialecki@polsl.pl

Abstract

The paper presents two techniques for obtaining spatial distribution of the heat transfer coefficient (HTC) for the impingement jet heat exchange problem. The former is an inverse one, which requires solution of the conduction problem in the object targeted by a jet. The HTC at the surface impinged by a jet is reconstructed directly from transient temperature measurements performed at the back surface of the object. A special formulation of the objective function allows for bypassing the nonlinearity of the underlying problem what significantly reduces computing time. The latter technique is the direct conjugate analysis. It involves solution of the temperature field in the object together with the flow and temperature fields within the jet and its surrounding. This technique gives more detailed solution, but is more time consuming and difficult to perform. Additionally the solution strongly depends on the turbulence model that closes the solved system of equations. The results of both presented approaches, for several geometrical configurations, are compared with the temperature readings from the infrared camera.

Keywords: inverse analysis, boundary conditions, jet impingement,, turbulence, CFD

1. Introduction

Jet impingement is a method of intensifying heat exchange. It involves a jet flow from a nozzle to a targeted surface [1]. The destruction of the boundary layer by the momentum of the fluid leads to high, local and surface averaged, heat transfer coefficients. Cooling of crucial parts of car and aircraft engines, turbine blades and electronics, are just few examples where impingement cooling is employed. Practical application of this technique requires a development of tools for predicting the intensity of the energy transfer at the impinged surfaces.

The inverse method [2] presented here allows for retrieving the BC's on the impinged surface by resorting to the superposition principle to build the heat conduction model. Then the simultaneous minimization of discrepancies resulting from retrieving the boundary flux and temperature as well as enforcing the constancy in time of the HTC coefficient is done. The current study investigates a spatial distribution of the heat transfer coefficient for a single phase air jet. It presents the retrieval of the HTC, by an inverse procedures, for several different nozzle diameters in order to verify the so-called effective heat exchange area for each situation. The inverse algorithm is implemented in the authors' in-house code with the least square fitting of the mathematical model and measurements performed using a modified Levenberg-Marquardt method. This technique provides additional regularization allowing for reduction of the influence of the ill-posedness of the inverse problem on the results. The sensitivity coefficients required for the evaluation of the model temperatures were computed using MSC.Marc, a commercial FEM code.

The direct analysis is performed in commercial code Ansys/Fluent. The conjugate approach is aimed at validating the assumption of the inverse technique and to find the most appropriate turbulence model for the impingement jet simulation. As the geometry and boundary conditions are axisymmetric the dimensionality of the analysis is reduced what diminish the necessary computing time.

2. Experiment

The single phase jet impingement experiment was carried out on the test rig schematically presented in Fig. 1. The heated object, is a steel disk made of made of OH18N9 stainless steel of

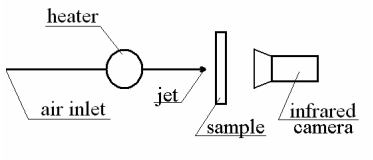

Figure 1. Scheme of experimental rig.

diameter d = 60.02mm and thickness h = 5mm. The thermal conductivity, density and specific heat are provided by manufacturer and equal to 16.2 W/(mK), 8000 kg/m^3, 500 J/(kgK) respectively. The sample is mounted in a PVC tube which screens its back sample against radiative heat exchange with surrounding objects. The tube is placed in a plate made of foamed polystyrene which insulates the side boundary of the sample. The use of the infrared camera for measuring temperature requires a technique of reducing the amount of data. At each camera frame produces about 8000 sensor readings which belong to the sampled area, which is far too much to be processed in the inverse analysis. The reduction of the number of measurements has been accomplished by taking advantage of the axisymmetry of the field. The radius of the sample is divided into equally spaced rings. Average temperature of all pixels within a given ring was assigned to the mean radius of the ring. The number of rings, equal to 21, was determined during the tests (see Fig. 2).

The nozzle is placed on the rail which align it coaxially with the sample and allows for setting the desired distance to the sample (see Fig. 3). The compressed ambient air flows to an electrical heater, where it is heated up to 340 K. In the initial phase of the experiment the air heats up all pipes and nozzle. The jet released from the nozzle does not impinge the disk but the screen

*The work was supported by the Polish Ministry of Science, Grant no. 3549/B/T02/2009/37

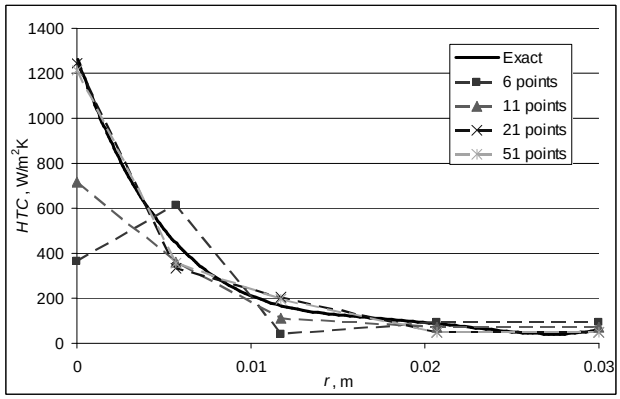

Figure 2. Influence of the amount of sensors on the HTC distribution.

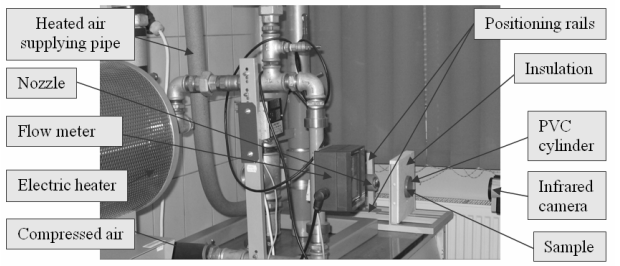

Figure 3. Influence of the amount of sensors on the HTC distribution.

which protects the disk from heating up before the steady state is reached. When the temperature of the heated air does not change, the steady state is achieved and then the infrared camera, placed 20cm from the back surface of the disk, starts recording thermograms. Then the screen is removed and the air starts impinging the sample. As seen in the images recorded by the camera, when the screen is removed the thermogram with a time $t = 0$ can readily be recognized. The hot air impinges the front surface and the sample starts heating up. The temperature measurements are taken using a SC-2000 infrared camera on the back surface of the sample. The images are recorded every 0.2 seconds. The experiment is conducted for three nozzle diameters d equal to 5, 6 and 7mm. Two distances l between the outlet of the nozzle and the sample are considered: 5d and 10d, where d stands for the diameter of the nozzle. The interval of time sampling was selected as 1s and the total time of data acquisition was taken as 30 seconds as after this time the changes of the temperature field were small.

The inverse analysis requires that the BC is known everywhere except at the impingement surface. The side surface of the disk is insulated as the disk is mounted in a foamed polystyrene plate. The back surface of the disk is not insulated, because the infrared camera needs a visual access to this surface. The back surface of the sample is in contact with the ambient air and it is cooled down by a natural convection and radiation. Those heat losses are neglected due to short time and small temperature difference and the surface is treated as insulated.

For all measurements the flow of air is adjusted to maintain constant Reynolds number equal to 22000 calculated with respect to nozzle diameter.

An important issue involved with all measurements is its uncertainty. It depends on four uncertainties coming from: direct measurement, object emissivity, temporal thermogram association and sensor location. The total uncertainty of the temperature field measurement is determined from a law of propagation of error [3] and is equal to 0.35K. This uncertainty is in the range of the stability provided by the numerical tests.

3. Developed technique

The reconstruction of the HTC is always pursued through the BCs of the 1st and 2nd kind. Therefore, the application of the developed technique to problems of unknown boundary flux and unknown temperature will be discussed first.

3.1. Procedure of retrieving the heat flux and temperature.

The heat flux is retrieved assuming that a linear problem is defined in a domain Ω bounded by a surface Γ. The boundary of the domain is divided into two parts. First part denoted as Γ_E where BCs are known and Γ_R where the heat flux is to be found (see Fig. 4).

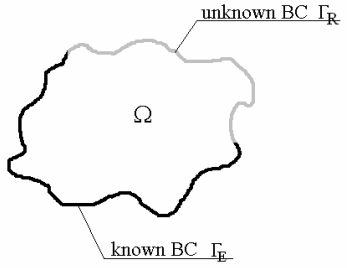

Figure 4. Domain of interest.

Applying the superposition principle the temperature field, depending on position $\mathbf{r}$ and time t can be expressed as a sum of two auxiliary fields:

$$T(\mathbf{r},t) = T_E(\mathbf{r},t) + T_R(\mathbf{r},t); \quad \mathbf{r} \in \Omega, t > 0 \tag{1}$$

The temperature field T_E corresponds to all known BCs, known initial condition and homogeneous heat flux i.e. $q = 0$ on Γ_R. The second temperature T_R corresponds to actual heat flux on Γ_R and homogeneous initial condition and all BCs on Γ_E. The term homogeneous BC means that for Dirichlet condition the temperature is equal to zero, for the Neumann condition the prescribed heat flux is zero while for the Robin condition, the HTC remains intact, while the free stream temperature T_f equals to 0. The unknown heat flux is approximated by a known set of K spatial and U temporal trial functions

$$q_R(\mathbf{r},t) = \sum_{k=1}^{K}\sum_{u=1}^{U} q_k N_k(\mathbf{r}) M_u(t) \tag{2}$$

To simplify the notation an index p defined as $p=K(u-1)+k$ is introduced. The index corresponds to a product of the k-th spatial and u-th temporal trial function. The approximating functions are chosen so their maximum value is one. The definition of the trial functions analogous to that used in FEM means also, that q_p can be interpreted as the values of the heat flux at association nodes. Therefore, the temperature T_R can be expressed as a sum of auxiliary fields Θ_p multiplied by the values of unknown heat fluxes q_p where Θ_p is a temperature field obtained solving a direct problem with homogeneous BCs on Γ_E and zero initial condition. The superposition principle applied to the temperature field leads to a formula containing searched approximation coefficients

$$T(\mathbf{r},t) = T_E(\mathbf{r},t) + \sum_{p=1}^{P} q_p \Theta_p(\mathbf{r},t) \tag{3}$$

Equation (3) is valid for arbitrary location and time and thus it is valid for the sensor locations $\mathbf{r}_i$ and moments t_s where the measurements have been acquired

$$T(\mathbf{r}_i,t_s)=T_E(\mathbf{r}_i,t_s)+\sum_{p=1}^{P}q_p\Theta_p(\mathbf{r}_i,t_s) \tag{4}$$

Such definition of the trial functions has one more advantage. Namely, the auxiliary temperature field Θ_p is in fact the sensitivity coefficient *j* computed with respect to the value of the unknown heat flux q_p at given location $\mathbf{r}_i$ and for time instant t_s. As for each combination of sensor location and time instant, only one value is measured, and for every spatial location the same number of measurements is taken, a subscript $z = I(s-1)+i$ running through all measurements is introduced.

$$j_{vp}=\frac{\partial T(\mathbf{r}_i,t_s)}{\partial q_p}=\frac{\partial T_v}{\partial q_p}=\{\mathbf{J}\}_{vp}=\Theta_p(\mathbf{r}_i,t_s) \tag{5}$$

The evaluation of the temperature field Θ_p a commercial MSC.Marc package have been used. Using this tool allows for handling any arbitrary geometry and BCs on Γ_E.

To determine the unknown fluxes q_p the temperatures calculated from the model are compared with the measurements. Sum of squared residuals written for every product of spatial and temporal function at all points *z* yields the objective function

$$\min_{w.r.t.\mathbf{q}}\Phi^q=\sum_{v=1}^{V}[\hat{T}_v-T_v{}^q(\mathbf{q})]^2=[\hat{\mathbf{T}}-\mathbf{T}_E^q-\mathbf{J}^q\mathbf{q}]^2 \tag{6}$$

where superscript *q* denotes heat flux retrieval and $\hat{\mathbf{T}}$ is a vector collecting all measured temperatures.

This optimization problem is recast into as solution of a set of linear equations by resorting to the necessary conditions for minimum. This se of equations is solved iteratively for the unknown vector of heat fluxes **q**. The entries of the Jacobian are just sampled values of the known and invariable auxiliary temperature fields Θ_p. Thus, the advantage of the present formulation is that direct solver is not invoked within the iterative loop. Moreover, the Jacobian of the system (5), whose values are necessary to use the efficient gradient based optimization solvers, is evaluated outside the iterative loop. Thus, the cost of the inverse method is small. Moreover, the sensitivity coefficients for a given set of functions may be computed once and stored in a file. They can be used many times, if only the geometry of the domain and the set of trial functions remain unchanged.

Both the temperature and heat flux retrieval problems are linear and the inverse algorithm can take advantage of the superposition principle. Therefore, the procedure of retrieving the boundary temperature is completely analogous to already described case of evaluation of the heat flux. It leads to nearly identical optimization formula

$$\min_{w.r.t.\mathbf{T}}\Phi^T=\sum_{v=1}^{V}[\hat{T}_v-T_v{}^T(\mathbf{T})]^2=[\hat{\mathbf{T}}-\mathbf{T}_E^q-\mathbf{J}^q\mathbf{T}]^2 \tag{7}$$

3.2. Procedure of retrieving the heat transfer coefficient.

A standard inverse technique of retrieving HTC could start with an approximation of the HTC using the concept of trial functions so the procedure would be analogous to the previously described. However, the dependence of the temperature field on the HTC is nonlinear so that the superposition principle cannot be used and moreover the sensitivity coefficients depend on the solution. This means that a direct problem solver and Jacobian evaluation procedure should be invoked at every step of the iterative minimization of the least squares functional. As the determination of the sensitivity coefficients takes over 90% of whole computing time, it is a serious drawback. The proposed inverse technique aims at circumventing this difficulty. There are two ways of accelerating the inverse procedure. Both of them relay on the application of the Newton cooling law

$$h_{k,u}=q_{k,u}/(T_f-T_{k,u}) \tag{8}$$

This formula allows for expressing the unknown HTC as a function of the retrieved heat flux and boundary temperature. If the definition of the Robin BC is introduced after the temperature and flux are retrieved the technique is called *implicit*. The definition of the trial functions ensure that the obtained approximations of temperature and heat flux are continuous in space and time. However, as the temperature and heat fluxes are retrieved independently, the HTC calculated for a given location *k* varies in time. As a result, the HTC is different at the beginning and the end of each time interval

$$h_{k,1}\neq\ldots\neq h_{k,U-1}\neq h_{k,U}\ \text{ for } u=1,\ldots,U \tag{9}$$

To produce constant values, time average HTC are determined. However, the physical correctness of such a procedure is doubtful.

The constancy in time can be achieved using the proposed *explicit* technique. Here, the Newton cooling law is used before the temperature and heat flux are known. In this case the HTC is a decision variable in the optimization formula. The first step of the algorithm is the reformulation of the least squares algorithm. The functional minimizes the discrepancy of the modeled and measure temperature and heat flux. This is achieved by summing up the functionals arising in the problems of retrieving the boundary heat flux (6) and temperature (7) and can be written as

$$\min_{w.r.t\,\mathbf{h},\mathbf{T}}\Phi=\sum_{v=1}^{V}[\hat{T}_v-T_v{}^T(\mathbf{T})]^2+\sum_{v=1}^{V}[\hat{T}_v-T_v{}^q(\mathbf{q})]^2 \tag{10}$$

In the next step, the heat flux is eliminated from the functional by resorting to the Newton law of cooling (8) (Robin's boundary condition). At this point the HTC at a given location is enforced to be constant. Finally, the minimized functional takes a following form

$$\min_{w.r.t\,\mathbf{h},\mathbf{T}}\Phi=\sum_{v=1}^{V}[\hat{T}_v-T_v{}^T(\mathbf{T})]^2+\sum_{v=1}^{V}[\hat{T}_v-T_v{}^q(\mathbf{T},\mathbf{h})]^2= \tag{11}$$
$$=[\hat{\mathbf{T}}-\mathbf{T}_E^h-\mathbf{J}^h\mathbf{a}]^2$$

where vector **a** contains values of both temperatures and HTC.

This not only reduces the number of unknowns but also improves the stability of the algorithm. The price to pay is a more complex Jacobian definition and more unknowns in the objective functions. Minimization of (11) is accomplished using the already described approach utilized when retrieving the boundary heat flux or temperature. The searched temperatures and the HTC are found in the least square sense which leads to the overdetermined set of equation. The set to be solved is twice times bigger than in the case of temperature or heat flux retrieval. The double amount of equations comes from summation of the two functionals. The vector of unknowns a consists of two parts of different lengths. The first part contains *k*u* temperatures while the second part *k* values of the HTC.

3.3. Validation procedure.

There are three techniques that allow for checking the quality of the solution of the inverse problem. The first one is the behavior of the vector of retrieved unknowns. The values of

the retrieved BC allows for judging the physical correctness of the solution, i.e. if the temperature increases in time or the heat flux or HTC decrease with the distance from the impingement area. It is important to see whether the physical constrains are fulfilled, but it will not quantify the accuracy of the solution. Thus, two more measures of the quality of the solution are introduced.

The first uses the value of the objective function Φ returned by the optimization solver along with the optimal values of the decision variables i.e. q_p or T_p for the *implicit* or T_p and h_p for the *explicit* scheme. The smaller the value of the objective function is, the better the approximation fits the measurements. For different tests, different number of equations corresponding to the number of measurements Z is solved. To compare two cases an average value of the objective function being the measure of the mean distance between the measurements and the approximation is considered

$$\Phi_Z = \frac{\Phi}{Z} \tag{12}$$

The second, is a posteriori technique of assessing the quality of the inverse solution. It requires an addition run of the heat conduction solver. The idea is, that once the distribution of the HTC is retrieved, all unambiguity conditions are known. Thus, the heat conduction problem can be solved directly. The geometry, material properties and numerical mesh are identical with those used for the genuine inverse analysis. The temperatures from the check run are then compared with the measurements for all sensor location $\mathbf{r}_i$ and times t_s. The RMS value of temperature discrepancies given as

$$RMS_{error} = \frac{\sqrt{\sum_{v=1}^{V}(\hat{T}_v - T_v)^2}}{V} \tag{13}$$

is then taken as a measure of the quality of the solution. This value is expected to be less or at least equal to the assessed temperature uncertainty (measurement error), greater value would implicate an unstable result.

The selection of the best solution requires checking of two criteria. The first criterion is the value of the objective function Φ_Z. The significantly different distributions of the HTC may produce similar values of the objective function. Therefore, not a single result but all solutions fulfilling

$$\Phi_Z \in (\Phi_{z\min}, 1.1\Phi_{z\min}) \tag{14}$$

are considered as potentially the best. Out of them the one which gave the least RMS temperature error from the check run of the inverse procedure is selected.

3.4. Conjugate analysis.

Even the simplest, submerged single phase jet, direct conjugate simulation requires careful selection of the turbulence model. For more complex configurations involving two phase flow, phase change etc., CFD does not offer reliable models. The aim of this simulation is to validate the main assumption of the inverse model. The crucial assumption made is the invariability of the HTC in time. Secondary purpose of the conjugate analysis is to test the performance of various turbulence models in reproducing both physics of the jet and the heat exchange associated with the impingement. The analysis was conducted in Ansys/Fluent, a commercial package with Gambit used as a preprocessor. All of the commonly used in practice turbulence models form the simplest k-ε to the RSM which are implemented in Ansys/Fluent were applied to the same case and compared to measurements and the findings of the inverse analysis. One have to keep in mind that the conjugate analysis requires couple of weeks (simple k-ε) to produce the results, while for the inverse analysis it is a matter of hours. However, if the HTC is constant in time and the aim of the analysis is to find its spatial distribution the time required for the conjugate analysis can be significantly reduced. In that case only the initial time of the phenomenon have to be simulated. Namely, the analysis has to be performed from the moment of the impingement to an occurrence of the fully developed velocity field. This time depends on the geometrical configuration but is in the range of 1s. The analyses conducted in this thesis considered much bigger time interval as the temperature field, at the back side of the sample, had to be compared with the measurements. Thus the simulated time was chosen as 8s.

The case at hand involves air jet released from the 5mm nozzle located at the distance of 5 nozzle diameters from the targeted object. As the geometry and BC's are axisymmetric and the influence of the gravity on the solution is negligible, problem is treated as axisymmetric. Thus, only 2D geometry have to be generated. The geometry with prescribed BC's is shown in Fig. 5. To obtain fully developed flow, part of the air supplying pipe has to be included in the model together with the part of the air surrounding the targeted object.

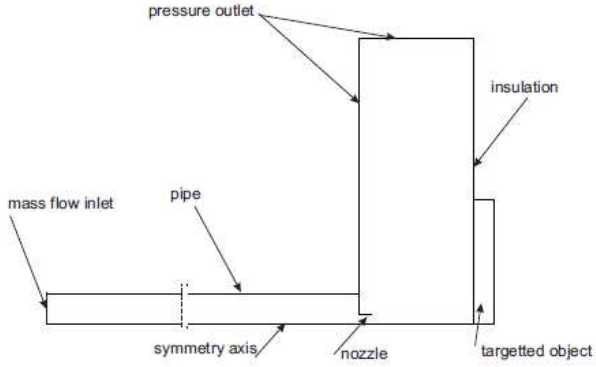

Figure 5. Computational domain.

To capture the effect of a boundary layer destruction by the momentum of the jet as well as the velocity changes in the impinged region, very fine mesh has been created in the vicinity of the stagnation zone and along the impinged surface of the sample. Additionally, the turbulence models required creation of the so called boundary layer to fulfill the $y+ < 1$ condition. The mesh size growths further from the sample and reaches its maximal size near the outlet condition. The final size of the mesh was determined during the mesh independence tests. As a result of those tests, a quadrilateral mesh consisting of 150k elements was created (see Fig. 6).

The conjugate flow and heat analysis is solvable only if closure equations modelling the turbulence are appended to the conservation equations of mass, momentum and energy. Several turbulence models are implemented in the Ansys/Fluent package used in this research. Numerous recommendations concerning the turbulence model appropriate for modelling jet impingement have been found in the literature. Additionally, the recent version of the Ansys/Fluentr package two new models designed for the transition flows are introduced. To investigate the differences between the available models all of them were tested for the same experimental setup. The only omitted model is the Spalart-Allmaras equation which is not relevant to the considered case. Some turbulence models, offer the possibility of using the wall functions to model the near wall region. The fine mesh present in the vicinity of the impinged surface forces

enabling the enhanced wall treatment (EWT) whenever this option is present.

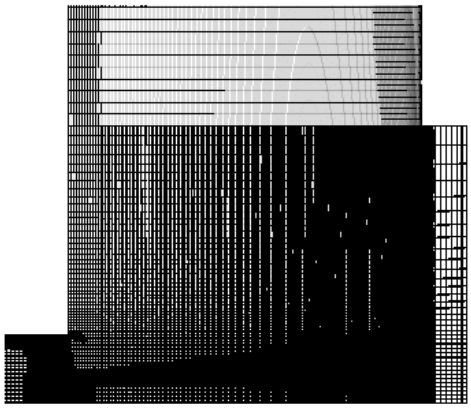

Figure 6. Numerical mesh.

4. Results

4.1. Conjugate analysis.

The results of the conjugate analysis show, that the HTC is constant in time for the impingement heat exchange, for all except of the k-kl-ω model. A sample results, obtained for the realizable k-ε model, are given in Fig. 7.

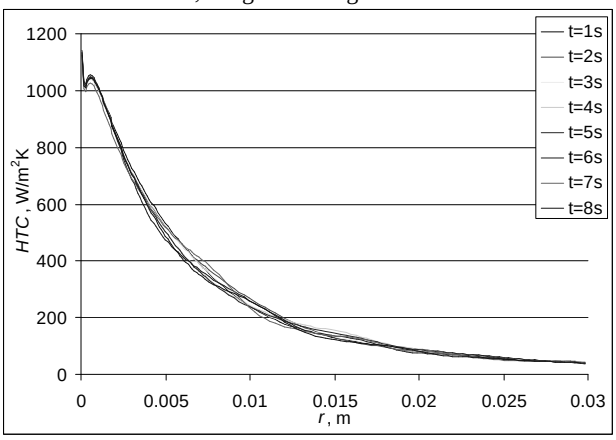

Figure 7. Distribution the HTC for various time instants.

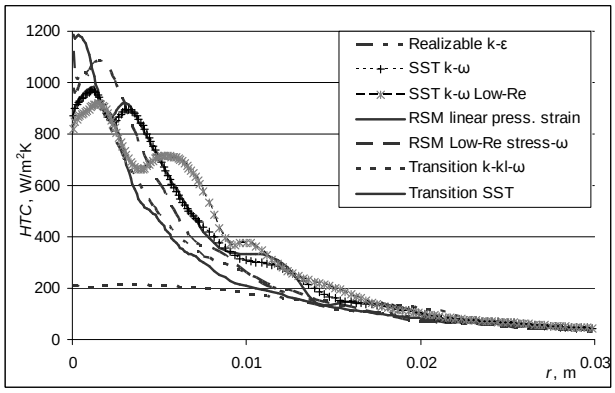

Figure 8. Reconstructed spatial distribution of the HTC.

The CFD simulation justified the introduction of the *explicit* scheme in the inverse algorithm. The spatial distribution of the HTC, presented in Fig. 8, shows that the result strongly depends on chosen turbulence model. Thus the accuracy of the HTC distribution obtained by any of those models is also doubtful. To select the most appropriate model, the RMS temperature differences for all 21 points distributed evenly along the radius of the sample and whole considered time interval was calculated. The comparison for the most important point i.e. the stagnation point are depicted in Fig. 9.

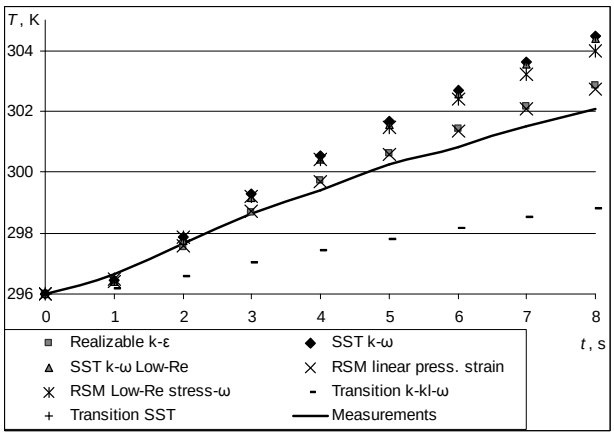

Figure 9. Comparison of the temperatures at a stagnation point.

Additionally, one have to notice, that the conjugate analysis did not produced conclusive results i.e. non of the models reproduced the measured temperatures correctly for the entire radius. Out of the tested turbulence models the RSM with linear pressure strain and the k-ε achieved the best overall agreement with the measurements. As the former is less computationally demanding, it will be used for all other geometrical configurations.

4.2. Inverse analysis.

The spatial distributions obtained for nozzle d=7mm located 5 diameters away from the impinged object are depicted in Fig. 10. Both inverse algorithms produced results marked by the least Φ_Z and RMS error for two temporal functions and the shortest temporal interval equal to 4s. The *explicit* scheme result is obtained for five while the *implicit* for four spatial functions.

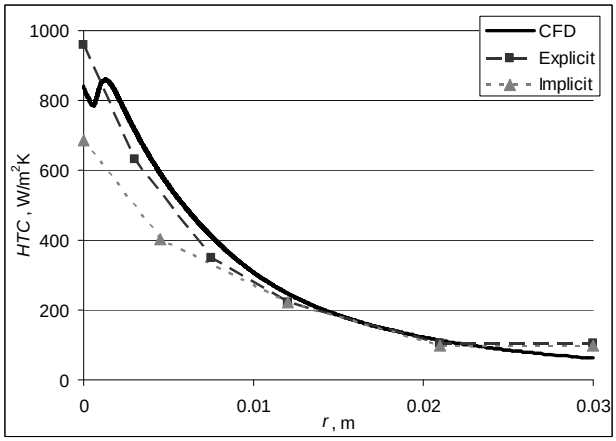

Figure 10. Spatial distributions of the HTC for 7mm nozzle located l=5d from the object.

For r > 8mm results are identical and very close to the direct simulation. For smaller radial coordinate the *implicit* scheme produces values lower by 20% than the *explicit* one. Both schemes produced different peak value of the HTC than their

conjugate counterpart. While the objective function values for both schemes, shown in Table 1 are identical, the RMS temperature errors are 40% bigger for the *implicit* scheme. This means, that the overall agreement for the explicit scheme is better.

Table 1. Value of the objective function and RMS temperature error for d=7mm l=5d

	$\Phi_{Z,K}{}^2$	*RMS error*
Implicit	0.026	0.035
Explicit	0.026	0.027
CFD	-	0.075

For the 7mm nozzle placed 70mm far from the steel disk, the peak value of the HTC predicted by both inverse schemes is bigger by about 30% than the predicted by conjugate simulation (see Fig. 11). The best spatial distributions of the HTC in terms

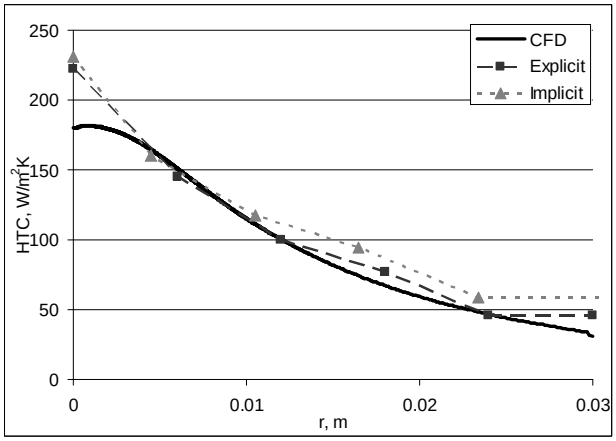

Figure 11. Spatial distributions of the HTC for 7mm nozzle located l=10d from the object.

of the objective function and RMS temperature errors are obtained for five spatial and three temporal functions extend over 8s time interval. The shape of both splines are very similar for r<0.012mm. For greater radial coordinate the *implicit* scheme produces slightly higher values. Again here, the values of the objective function (see Table 2) are nearly identical, while the RMS error is much higher for the *implicit* scheme.

Table 2. Value of the objective function and RMS temperature error for d=7mm l=10d

	$\Phi_{Z,K}{}^2$	*RMS error*
Implicit	0.029	0.421
Explicit	0.031	0.032
CFD	-	0.068

As the result of the inverse algorithms are very close to one another, the reason behind this difference in RMS temperature error is the temporal variation of the result for the *implicit* scheme.

For all tested nozzle diameters d and nozzle to object distance l the results obtained from the inverse schemes exhibit good agreement with the findings of the direct conjugate analysis. Generally, the *explicit* scheme predicts HTC distribution closer to the direct simulation than the *implicit* one. Thus, the results of this scheme are compared to the CFD results below. In the case of the nozzle located close to the sample (see Fig. 12), the retrieval quality is very good for the smallest and the largest nozzle. For the 6mm nozzle the HTC distribution seems to be underpredicted.

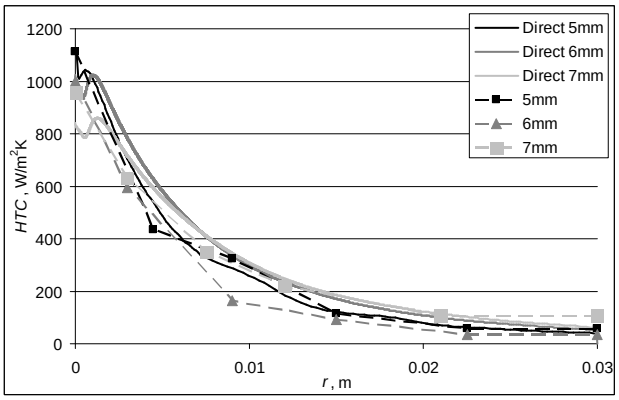

Figure 12. Spatial distributions of the HTC for 7mm nozzle located l=10d from the object.

The literature study [1], [4] revealed that the peak value of the HTC increases with the increase of the nozzle diameter up to l÷5 and decrease afterwards. The descent of the HTC with radial coordinate is higher for the smaller nozzles which implicates lower HTC for average radial coordinate. The HTC value for r > 4d does not depends on the nozzle diameter, but only on the Reynolds number. This behaviour is confirmed by the results of the direct analyses and all but one inverse analysis. Only the distribution obtained for the 6mm jet produce the lowest value for r≈0.01. For all nozzle diameters, the inverse analysis is unable to capture the presence of second extremum located near the stagnation zone. It can be explained by the fact that there is no possibility to put an additional spatial trial function in the vicinity of the secondary peak and maintain the stability of the scheme. Yet, both the magnitude and shape of the HTC distribution is well captured.

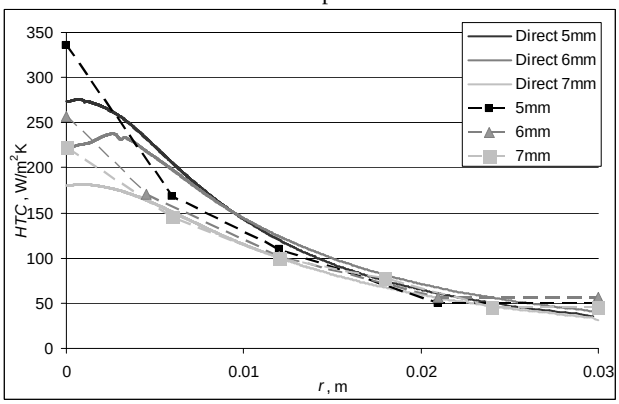

Figure 13. Spatial distributions of the HTC for 7mm nozzle located l=10d from the object.

For the second tested nozzle to sample distance l=10d the results are shown in Fig. 13. For all tested nozzle diameters, there are significant differences in the HTC in the stagnation zone. Namely, the HTC values predicted by the inverse procedure are higher than in the case of the direct conjugate analysis. For 5mm and 6mm nozzles the HTC decreases rapidly with the radial coordinate and for the second spatial function it is lower than the CFD prediction. This might indicate, that the peak value is overestimated while the one for second function underpredicted. Further from the stagnation point the HTC predictions are nearly identical for all nozzle diameters. The peak value of the HTC for both inverse and direct simulation decreases with the increase of the nozzle diameter which is in accordance with literature and common sense. The results for submerged jet shows superiority of the explicit scheme over the implicit one. Although, for some tested cases, the value of the

objective function is similar for both schemes, the RMS temperature difference for all configurations is smaller for the explicit one.

5. Conclusions

The results obtained for the submerged air jet together with conjugate analysis proved that the developed inverse technique can successfully be applied to retrieve the HTC distribution for various geometrical configurations and jet parameters. The spatial distribution is often retrieved for five spatial functions which allows for capturing both magnitude and shape of the HTC distribution. Yet, still the solution is smoothed by the approximation of both spatial and temporal trial functions involved in the inverse procedure and thus, some details of the variation of the function are lost. This can be observed especially for larger $l=d$ for air jet, where the extremum shifted from the stagnation zone is not reproduced by the inverse technique.

The temperature measurements are closer to the results of the inverse analysis than to that of the CFD simulations. It is important to notice that the inverse analysis does not retrieve the local maximum of the HTC. The attempt to approximate the HTC distribution using more functions placed in the stagnation zone failed to produce feasible results. Such a behavior is a common feature of the inverse procedures. The accuracy of the solution is always a compromise between the stability of the solution and the desired amount of information from the inverse analysis.

The most troublesome problem when in CFD simulations is the usage of proper turbulence model. Even for relatively simple single phase submerged jet the turbulence model plays crucial role in the simulation process. Besides, the computational time for the direct analysis is much higher than its inverse counterpart. Inverse analysis requires however temperature measurements and it is able to retrieve only low order approximation of the HTC distribution. Thus it flattens the HTC value in the stagnation region. As a result, the value of the HTC is under predicted. The temperature comparison shows very good agreement between the inverse results and the measurements. It shows that despite the fact that not all details are retrieved the general agreement is good for all nozzle diameters and nozzle to sample distances. Further development of the code is necessary to improve its stability and make possible to retrieve the HTC using higher number of functions.

References

[1] Stevens J., and Webb B.W., *Local Heat Transfer Coefficients Under an Axisymmetric, Single-Phase Liquid Jet*, J. Heat Transfer **113**, pp. 71-78 (1991)

[2] Özisik N. M. and Orlande H. R. B., *Inverse Heat Transfer Fundamentals and Applications*, Taylor and Francis, NY 2000.

[3] Woodbury K., editor. *Inverse engineering handbook*. CRC Press, Boca Raton, 2003

[4] Souris N., Liakos H., and Fonti M. Impinging jet cooling on concave surfaces. *AIChE Journal*, pp 1672–1683 (2004)